crystals

MDPI

Article

Electrodeposited Fabrication of CeO_2 Branched-like Nanostructure Used for Nonenzymatic Glucose Biosensor

Nguyen Thi Nguyet [1], Chu Van Tuan [1], Dang Thi Thuy Ngan [2], Phuong Dinh Tam [2], Vinh Dinh Nguyen [3] and Nguyen Trong Nghia [1,*]

[1] Faculty of Chemical Technology and Environmental, Hung Yen University of Technology and Education, Hung Yen 17817, Vietnam; nguyennguyet@utehy.edu.vn (N.T.N.); chuvantuan@utehy.edu.vn (C.V.T.)
[2] Faculty of Material Science and Engineering, Phenikaa University, Hanoi 12116, Vietnam; dangthithuynganhh@gmail.com (D.T.T.N.); tam.phuongdinh@phenikaa-uni.edu.vn (P.D.T.)
[3] Faculty of Chemistry, TNU-University of Sciences, Tan Thinh Ward, Thai Nguyen 25000, Vietnam; vinhnd@tnus.edu.vn
* Correspondence: nguyentrongnghia@utehy.edu.vn

Abstract: The fabrication of nonenzymatic glucose sensors is essential because of the enhancement in the selectivity and accuracy of these sensors. In this work, we used the electrodeposition approach to prepare a CeO_2-based electrode for nonenzymatic glucose detection. A CeO_2 branched-like nanostructure was successfully fabricated by electrodeposition on the surface of a Au substrate electrode at room temperature. The effects of cyclic voltammetry, CH_3COOH content, and scan cycle number on the formation of the CeO_2 branched-like nanostructure were investigated. The fabricated electrodes were characterized by scanning electron microscopy (SEM), energy-dispersive X-ray spectroscopy (EDS), X-ray diffraction (XRD), and Fourier transform infrared spectroscopy (FTIR). The results showed that a CeO_2 branched-like nanostructure could be obtained with a CH_3COOH content of 1.0 mL and a scan cycle number of 100 in a solution containing 0.015 M $Ce(NO_3)_3$, 0.01 M KCl, and 0.02 M CH_3COONH_4 and with a scan rate of 400 mV/s. The electrochemical characteristics of the sensor were examined by chronoamperometry and cyclic voltammetry. The results showed that the sensitivity of the sensor was 37.72 $\mu A/mM{\cdot}cm^2$ and the limit of detection (LOD) of the sensor was 0.093 mM. The findings in this work prove that it is feasible to fabricate CeO_2-based sensors for nonenzymatic glucose detection.

Keywords: nonenzymatic biosensor; CeO_2; branched-like structure; electrodeposition; glucose

Citation: Nguyet, N.T.; Tuan, C.V.; Ngan, D.T.T.; Tam, P.D.; Nguyen, V.D.; Nghia, N.T. Electrodeposited Fabrication of CeO_2 Branched-like Nanostructure Used for Nonenzymatic Glucose Biosensor. *Crystals* **2023**, *13*, 1315. https://doi.org/10.3390/cryst13091315

Academic Editor: Paolo Olivero

Received: 1 August 2023
Revised: 18 August 2023
Accepted: 21 August 2023
Published: 29 August 2023

1. Introduction

Diabetes is a common disease that dramatically affects the quality of life of millions worldwide. It has become one of the three leading causes of death in patients. Hence, the detection of glucose in blood can save lives and control the condition of thousands of people with diabetes. However, most commercial sensors today are still mainly glucose sensors that use the glucose oxidase (Gox) enzyme [1–6]. The use of enzymatic sensors requires a prolonged time for sample preparation, technical efforts, and a number of chemicals for immobilizing GOx on the sensor's surface. Enzyme-based sensors detect glucose through a variation in the electrical signal caused by either oxygen consumption or the production of H_2O_2 in the enzyme's response to glucose. This process requires a relatively high anodic potential, which can lead to the simultaneous oxidation of ascorbic acid and uric acid present in the blood, reducing the selectivity and accuracy of the sensor [7].

In contrast, the utilization of nonenzymatic sensors can shorten the sample preparation time and guarantee the enzyme storage conditions on the electrode surface of the sensor. In addition, using functional materials synthesized by different methods and then coating them on the sensor surface through basic methods such as the drip-drop or spin-coat

methods leads to an increase in resistance, hindering the charge transfer from the surface-layer functional materials to the sensor electrode. According to the report of Dae-Woong Hwang [8], the dendritic structures of functional materials indicate a higher ability to catalyze the oxidation of glucose in a solution.

CeO_2 is one of the rare earth oxides with good physical and chemical properties such as electrical conductivity, optical properties, and catalysis properties. Therefore, it has been widely used in various fields such as optical [9,10], energy storage [11,12], conductive materials [13,14], ultraviolet absorber materials [15,16], gas sensors [17,18], and biosensors [19–23]. CeO_2 is of great interest in biosensor applications due to its good redox properties caused by surface defects and oxygen vacancies [24]. Moreover, the surface area of CeO_2 can be enhanced by tuning its morphology. With its diverse morphology, CeO_2 is a perfect candidate for use as a carrier to load other materials. Sensors based on CeO_2 are mainly fabricated through several steps, such as synthesizing CeO_2 and fixing it on the electrode surfaces. However, the multi-step fabrication required reduces the electrical conductivity from CeO_2 to the electrode surface, reducing the sensitivity and the unique features of these electrochemical sensors. The direct electrodeposition of CeO_2 on the electrode surface is a promising approach to overcome this limitation because it can enhance the conductivity between the functional material (CeO_2) and the electrode surface. Moreover, one-step fabrication can shorten the time required for the sensor fabrication process and reduce the use of chemicals for fixing CeO_2 on the substrate. The electrodeposition of CeO_2 for biosensor application has been reported in several studies [9,25–28]. Accordingly, CeO_2 is mainly synthesized by a constant-current approach [9,25,27] or a constant-potential approach [26] at a relatively high temperature of 70 °C. However, these methods have drawbacks, such as a high energy consumption and a long fabrication time (from 60 to 120 min). Therefore, developing an effective alternative technique for the electrodeposition of CeO_2 is necessary for practical applications. The morphology of CeO_2 is also an important factor affecting its catalytic capability [29]. CeO_2 with a branched-like structure, which has some advantages such as a high surface area and a porous texture, could be a prominent catalyst for glucose sensors. However, to the best our knowledge, the use of a CeO_2 branched-liked structure for nonenzymatic glucose biosensors has been rarely reported.

The present work aimed to fabricate a nonenzymatic glucose sensor based on CeO_2 with a branched-like structure using the electrodeposition method. A CeO_2 branched-like structure was directly created onto the surface of an Au substrate electrode by the electrodeposition method in a solution containing $Ce(NO_3)_3$, KCl, CH_3COONH_4, and CH_3COOH at room temperature. The effects of the parameters, including the applied potential, acid content, and scan cycle number (SCN), were investigated. The feasibility of the fabricated sensor in detecting glucose was also examined.

2. Materials and Methods

2.1. Chemicals

All chemicals were analytical grade and used without further purification. Cerium(III) nitrate hexahydrate ($Ce(NO_3)_3 \cdot 6H_2O$, 99.999%), ammonium acetate (CH_3COONH_4, >98%), potassium chloride (KCl purity $\geq$ 99%), acetic acid (CH_3COOH, 100%), β-D-glucose ($C_6H_{12}O_6$, 98%), and sodium hydroxide (NaOH, ≥98%) were purchased from Sigma-Aldrich. All solutions were prepared with ultrapure water (18.2 MΩ·cm) obtained from a Millipore Milli-Q system.

2.2. Fabrication of CeO_2-Based Biosensors

The substrate electrode was 5 mm in width and 10 mm in length and was fabricated by sputtering Au onto a silicon dioxide/silicon substrate. A saturated Ag/AgCl electrode was used as the reference electrode, and a platinum plate was employed as the counter electrode. The electrodeposition experiments were carried out in a solution containing 0.015 M $Ce(NO_3)_3$, 0.01 M KCl, and 0.02 M CH_3COONH_4 and a certain amount of CH_3COOH

using the cyclic voltammetry method at room temperature with a cyclic voltammetry range of −0.4–1.8 V. According to our previous study [30], a scanning rate of 400 mV/s was the optimal value for electrodeposition of CeO_2 onto a Au substrate electrode. Therefore, in this work, a scanning rate of 400 mV/s was used.

2.3. Characterization

The morphology and chemical content of the fabricated materials were analyzed using a field emission scanning electron microscope (FE-SEM, JSM-7600F, Jeol, Tokyo, Japan). The X-ray diffraction (XRD) characterization was carried out using an XRD EQUINOX 5000 (Thermo Scientific, Illkirch-Graffenstaden, France) device with a monochromatized Cu, Kα radiation source with a wavelength of 0.154 nm. The Fourier transform infrared spectrum of the sample was recorded on an FTIR Affinity—1S equipment (Shimadzu, Kyoto, Japan).

2.4. Glucose Detection Test

Before measurement, the fabricated electrodes were cleaned using a 0.5 M H_2SO_4 solution and ultrapure water. All the measurements were conducted in a conventional three-electrode electrochemical cell with a Ag/AgCl reference electrode and a platinum counter electrode at room temperature. A PGSTAT Autolab 302N system (Metrohm Autolab–BV, Utrecht, Netherlands)) with the Nova 1.11 software (Metrohm Autolab–BV, Utrecht, Netherlands) was used to study the oxidation reaction of glucose on the surface of the biosensor. The chronoamperometry method was utilized to record the detection signal of the oxidation process of glucose in a 0.1 M NaOH solution at a potential of 0.45 V vs. saturated Ag/AgCl.

3. Results and Discussion

3.1. Cyclic Voltammetry Curves

Cyclic voltammetry is a technique commonly used in the electrodeposition synthesis of nanomaterials. It involves applying a potential to an electrode in a solution containing the desired precursor ions and measuring the resulting current as a function of the applied potential. By varying the potential over a range of values, cyclic voltammetry provides information about the electrochemical behavior of the system and allows for control over the deposition process. In this work, the experiment was performed with a potential range of −0.4–1.8 V and a scan rate of 400 mV/s in a solution of 0.015 M $Ce(NO_3)_3$, 0.01 M KCl, and 0.02 M CH_3COONH_4, and the results are given in Figure 1.

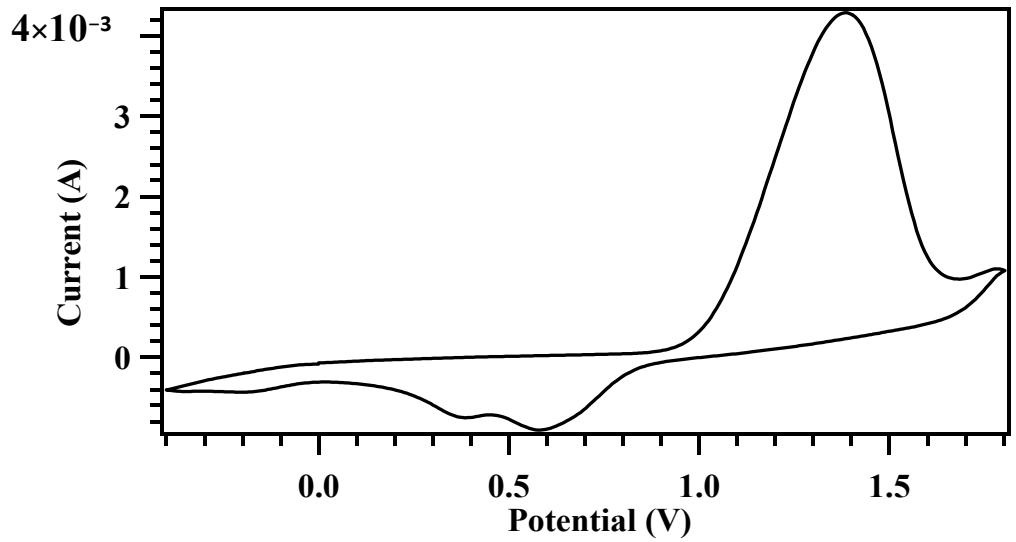

Figure 1. Cyclic voltammetry behavior of the deposition of CeO_2 with a cycle number of 10.

The experimental data showed that there were one anodic and two cathodic peaks. The anodic peak at a potential of 1.36 V corresponded to the oxidation of the Ce^{3+} ions to form CeO_2 on the surface of the substrate electrode as per the following equation:

$$4Ce^{3+} + O_2 + 12OH^- - 4e \rightarrow 4CeO_2 + 6H_2O \quad (1)$$

The cathodic peak at a potential of 0.59 V was due to the reduction of NO_3^- ions in the solution. This process can be presented as follows:

$$NO_3^- + H_2O + 2e \rightarrow NO_2^- + 2OH^- \quad (2)$$

There was another cathodic peak at about 0.38 V, which originated from the reduction of protons in the solution:

$$2H^+ + 2e \rightarrow H_2 \quad (3)$$

The diffusion coefficient of electrodeposition for CeO_2 is a specific parameter that characterizes the rate at which cerium ions or cerium-containing species move through a medium during the electrodeposition process of CeO_2. The diffusion coefficient was calculated using the Randles–Sevcik equation [31]:

$$i_p = -2.69 \cdot 10^5 \cdot n^{3/2} \cdot A \cdot D_o^{1/2} \cdot C_o \cdot v^{1/2} \quad (4)$$

where i_p is the current maximum (A), n is the number of electrons transferred in the redox reactions, A is the electrode area (cm^2), D_o is the diffusion coefficient (cm^2/s), C_o is the concentration, and v is the scan rate. The calculation showed that the diffusion coefficient was about $6.9 \cdot 10^{-7}$ cm^2/s, suggesting that the diffusion step controlled the reaction [32].

3.2. Effect of CH_3COOH Content

The presence of CH_3COOH in the solution played a vital role because it created an environment for the redox reactions to occur when cyclic scanning was performed. It was considered as the critical parameter for the formation of CeO_2 on the working electrode surface. For investigating the influence of the CH_3COOH content, the experiments were carried out with different volumes of CH_3COOH ranging from 0 to 1.5 mL in a 100 mL working solution. The results presented in Figure 2 reveal that the CH_3COOH content significantly affected the morphology of the CeO_2 formed on the electrode surface. The SEM image of the sample without CH_3COOH (Figure 2a) showed small particles formed on the surface of the electrode, while on that of the sample with 0.5 mL of CH_3COOH (Figure 2b), a branched-like structure of CeO_2 could be observed. This structure was clearly detected when the content of CH_3COOH was 1.0 mL (Figure 2c). When the added volume of CH_3COOH was increased to 1.5 mL, the branches became bigger and tended to form large blocks (Figure 2d). The effect of the CH_3COOH content on the morphology of the CeO_2 formed on the surface of the substrate electrode may have originated from the complexation of Ce^{3+} ions and CH_3COO^- ligands that stabilized Ce^{3+} in the solution and prevented the formation of Ce_2O_3 [33]. The CH_3COOH content also affected the pH of the solution, which probably impacted the nucleation and growth of CeO_2 crystals on the electrode surface. Consequently, it impacted the final morphologies of the products. Accordingly, the CH_3COOH content of 1.0 mL was proper for preparing a CeO_2 branched-like nanostructure on the surface of the Au substrate electrode.

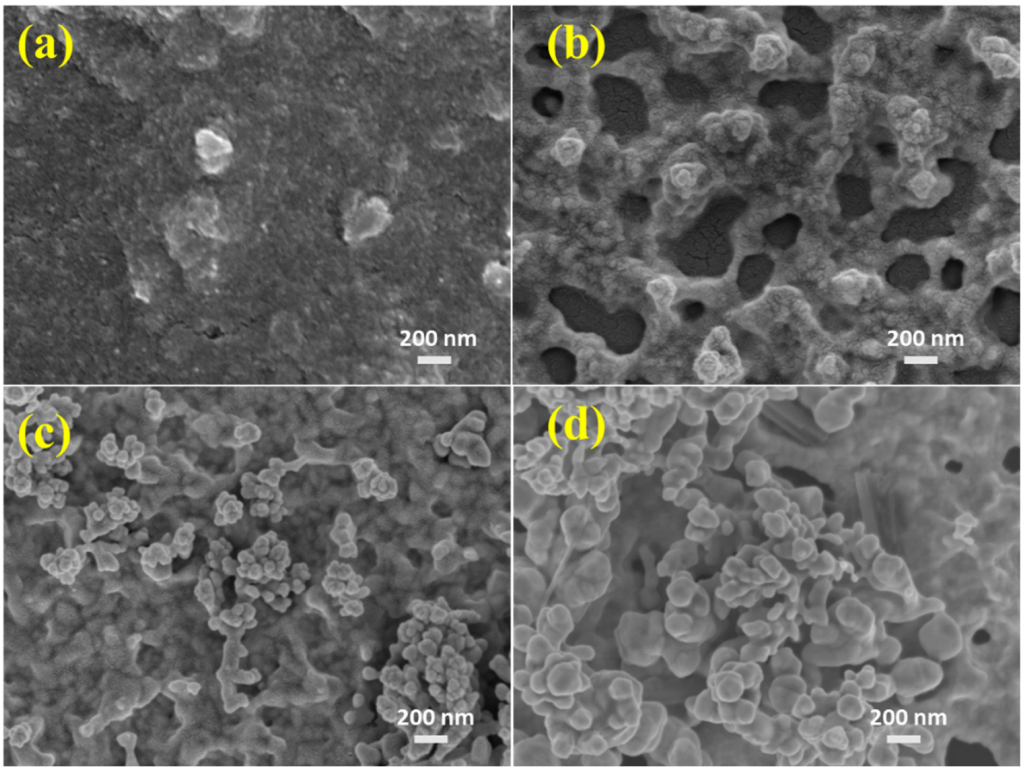

Figure 2. FeSEM images of CeO_2 obtained from solutions containing CH_3COOH: (**a**) 0 mL, (**b**) 0.5 mL, (**c**) 1.0 mL, and (**d**) 1.5 mL in 100 mL working solution.

3.3. Effect of Scan Cycle Number

The scan cycle number (SCN) is an important parameter that affects the electrodeposition process because it determines the duration and sequence of the applied potential. For studying the effect of the scan cycle number on the formation and morphology of CeO_2 on the surface of the substrate electrode, the experiments were carried out with different scan cycle numbers, from 10 to 200, and the results are shown in Figure 3. It can be seen that when the SCN increased from 10 to 100, the intensity of the anodic peak slightly increased. The highest intensity was obtained with an SCN of 100. When the SCN rose to 150 and 200, the intensity of the anodic peaks declined. The change in the intensity of the anodic peak with the increase in the SCN can be explained by the fact that with an SCN of 10, the deposition of CeO_2 on the electrode surface was difficult due to the overpotential of the oxidation of Ce^{3+} to form CeO_2 on the Au surface ($\eta_{CeO_{2/Au}}$). When the SCN increased to 50 and 100, the deposition was favorable because the deposition occurred on the CeO_2 film that was not affected by the overpotential $\eta_{CeO_{2/Au}}$. As the SCN was increased to 150 and 200, the concentration of Ce^{3+} declined, thus reducing the current intensity.

For investigating the effect of the SCN on the morphology of the CeO_2 on the electrode surface, the samples with different SCNs were analyzed using the SEM technique, and the results are given in Figure 4. It is clear that the morphology of the obtained CeO_2 significantly changed with the change in the SCN. A thin film can be observed for the sample with an SCN of 10 (Figure 4a), which consisted of only CeO_2 nanoparticles with a diameter of about 100 nm. As the SCN increased to 50, the CeO_2 nanoparticles were grown gradually to form a CeO_2 branched-like nanostructure on the gold electrode surface, as illustrated in Figure 4b. The branched-like nanostructure can be observed for the samples with an SCN of 100 and 200 (Figure 4c,d). These results indicated that a CeO_2 branched-like nanostructure could form on the Au electrode surface with an SCN of 100.

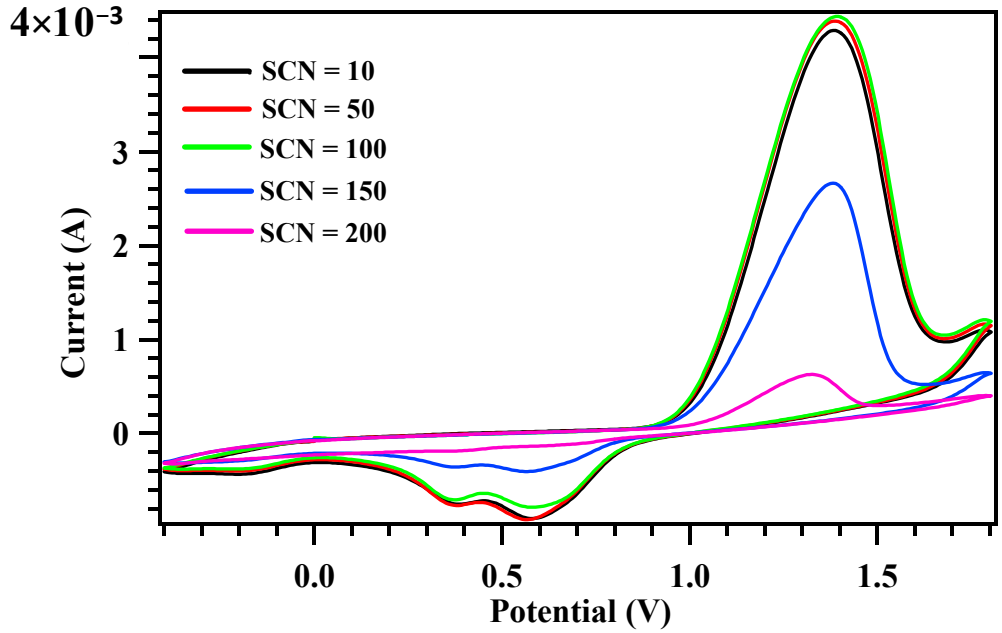

Figure 3. Cyclic voltammetry for the synthesis of CeO_2 with different SCNs and a scan rate of 400 mV/s at room temperature.

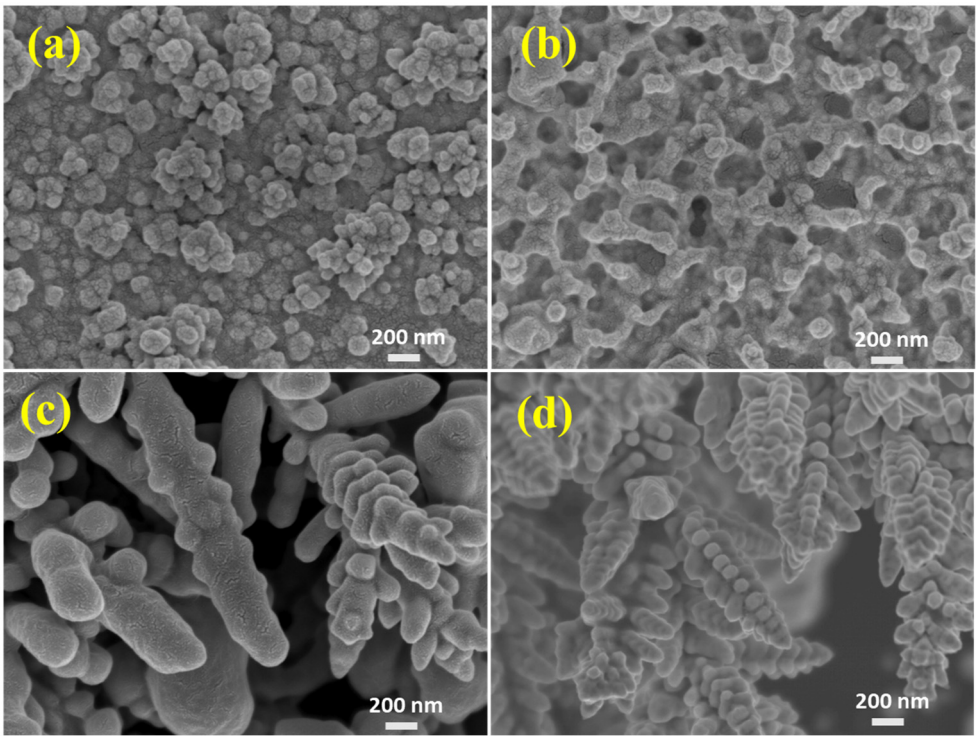

Figure 4. FeSEM images of the surface of the electrode: (**a**) SCN of 10; (**b**) SCN of 50; (**c**) SCN of 100; and (**d**) SCN of 200.

3.4. Electrode Characterization

The element content of the electrode surface was determined using energy-dispersive X-ray spectroscopy, and the analyzed data are given in Figure 5. The results indicated that the sample contained mainly O (34.24%), Ce (29.32%), and Au (277.56%). In addition, the presence of carbon in the sample was also observed, which may be due to the adsorption of CO_2 or the sample preparation process.

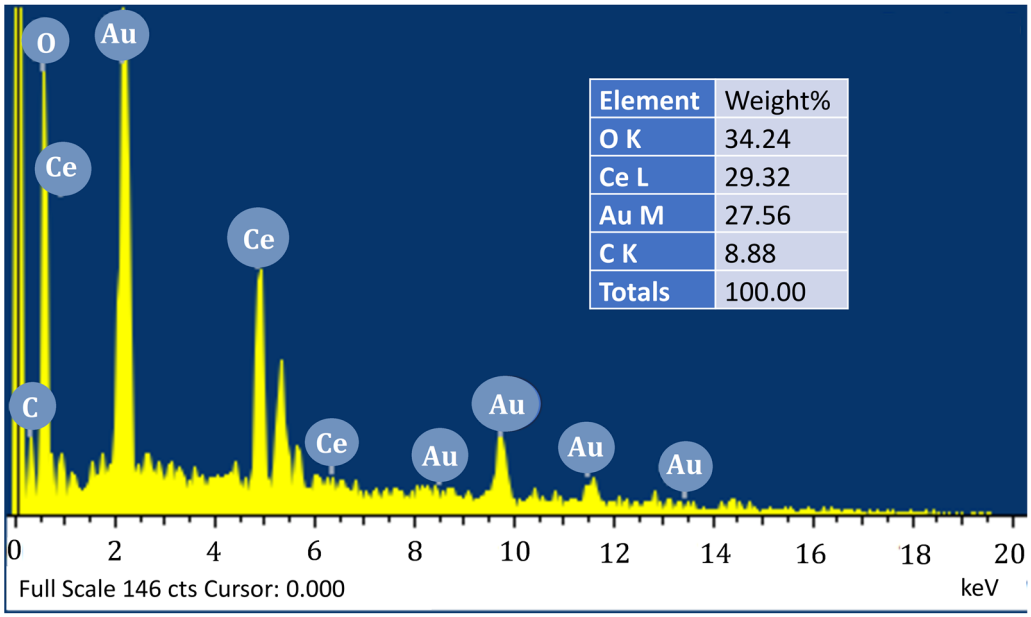

Figure 5. EDS analysis of the surface of the electrode based on CeO_2 branched-like nanostructure.

The crystalline phase contents of the fabricated electrode were determined using the XRD method, and the results are presented in Figure 6. On the XRD pattern, the diffraction peaks observed at the two-theta angles of 28.9, 33.6, 48.02, and 56.8° corresponded to the reflections of the (111), (200), (220), and (331) crystallographic planes of the fcc fluorite structure of CeO_2 (JCPDS 34-0394) [34]. In addition, the diffraction peaks at about 38.6 and 44.7° were due to the reflection of the (111) and (200) planes in the centered cubic (fcc) gold (JCPDS 89-3697). The XRD data indicated the formation of CeO_2 crystals on the surface of the Au substrate electrode.

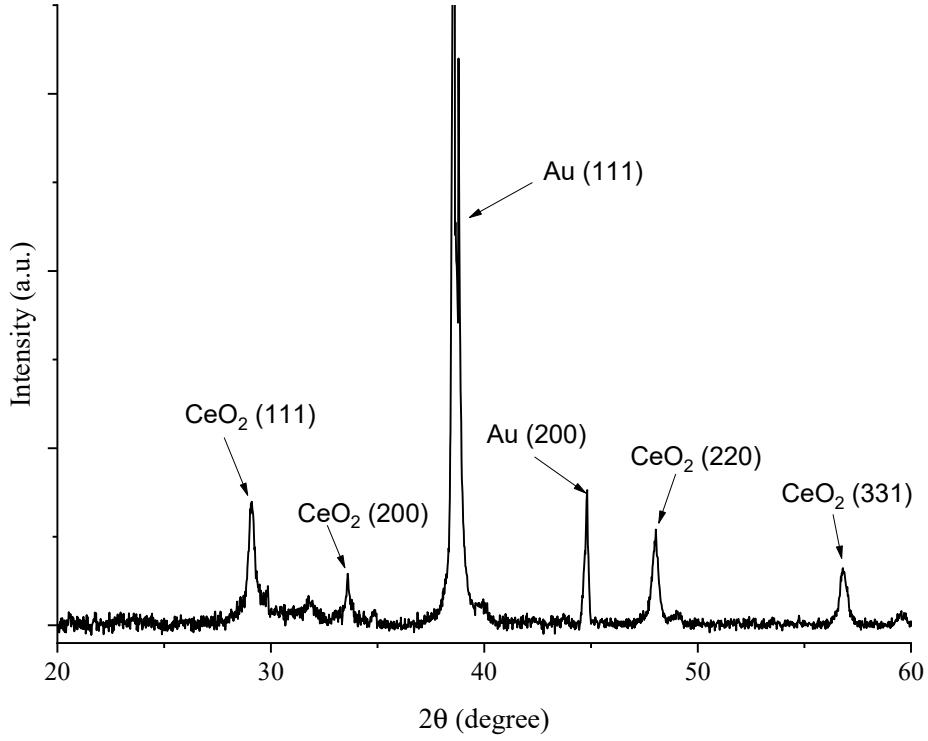

Figure 6. XRD pattern of the surface of the electrode based on CeO_2 branched-like nanostructure.

Figure 7 shows the FTIR spectrum of the fabricated electrode sample. There are several noticeable absorption peaks in the wavenumber range of 4000–500 cm^{-1}. Broad absorption peaks at about 3266 cm^{-1} were indexed to the stretching vibration of the –OH group in the water molecules. The peaks at 1579 and 1314 cm^{-1} were assigned to the water molecules that were physically adsorbed onto the surface. The peak in the range of 500–600 cm^{-1} was associated with the asymmetric and symmetric vibrations of Ce–O [35].

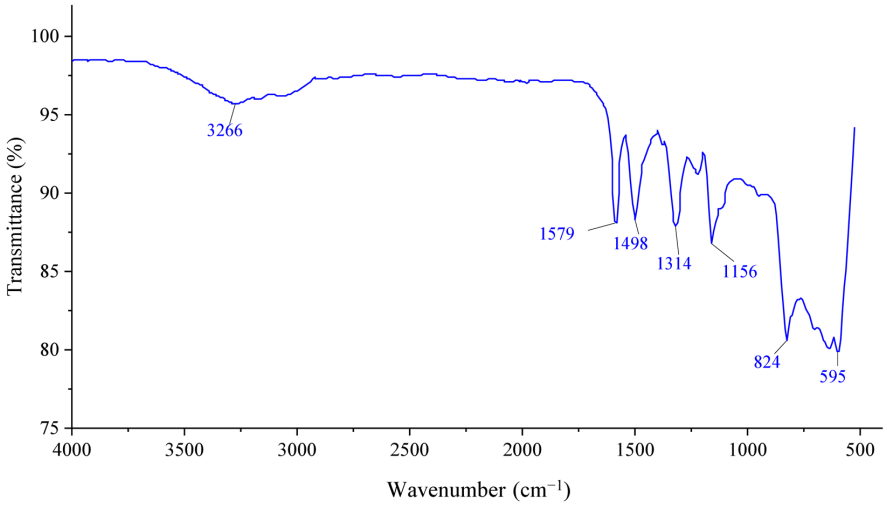

Figure 7. FT-IR spectrum of the electrode modified by CeO_2 branched-like nanostructure.

3.5. Feasibility for Nonenzymatic Glucose Detection

3.5.1. Determination of the Oxidation Potential of β-D-Glucose

To determine the oxidation potential of β-D-glucose, linear sweep voltammetry (LSV) was employed. The experiments were carried out using a potentiostat and a three-electrode electrochemical cell to transport a potential to a solution and screen its variation in current. Figure 8 shows the LSV voltammograms of the substrate electrode (Figure 8A) and the fabricated CeO_2-based electrode in the solutions of 1 M NaOH (black line) and 1 M NaOH + 10 mM β-D-glucose (red line). The data indicated that for the substrate electrode, there was not any oxidation peak on the LSV voltammogram, indicating that the oxidation process of β-D-glucose did not occur on the surface of the substrate electrode. In contrast, the LSV voltammogram of the fabricated CeO_2-based electrode shows an oxidation peak at about 0.45 V, corresponding to the oxidation potential of β-D-glucose. These results indicate that the electrode fabricated by the electrodeposition of CeO_2 onto the substrate electrode's surface could be used to detect the β-D-glucose in the solution.

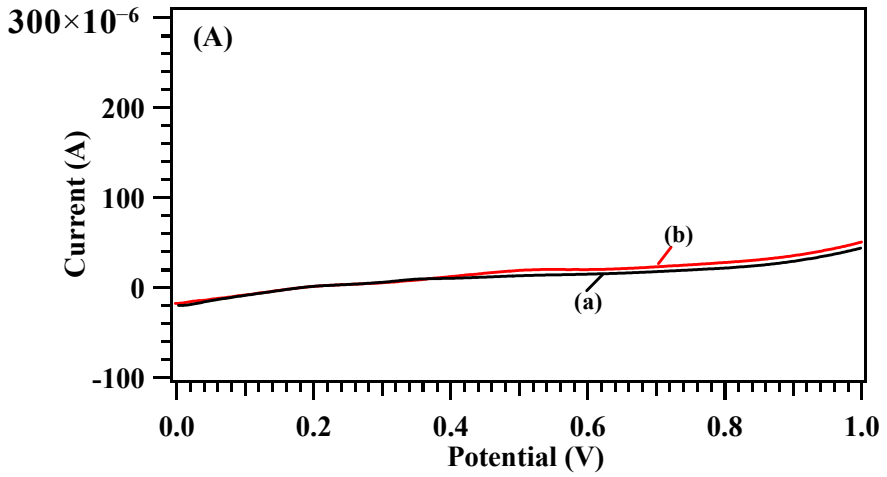

Figure 8. *Cont.*

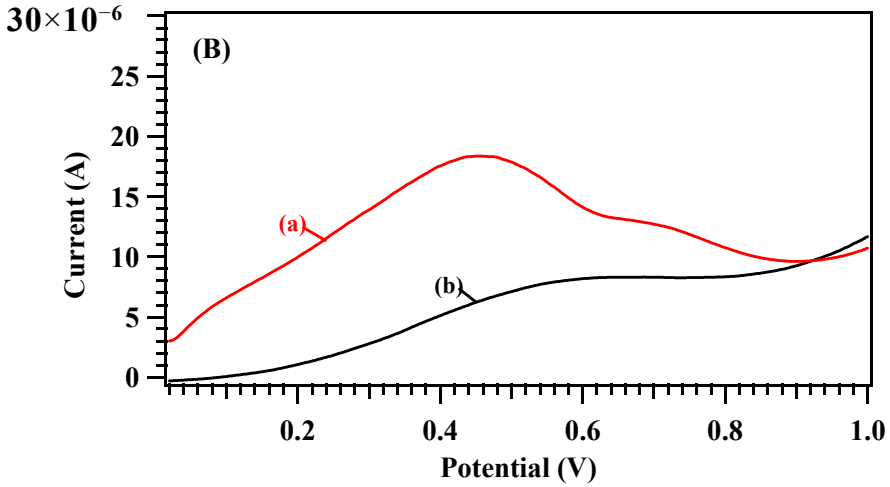

Figure 8. LSV voltammograms of: (**A**) bare Au electrode in (a) 1 M NaOH solution and (b)—1 M NaOH + 10 mM β-D-Glucose, and (**B**) electrode based on CeO_2 branched-like nanostructure in (a) 1 M NaOH solution and (b) 1 M NaOH + 0.02 mM β-D-glucose solution.

3.5.2. Electrochemical Detection of Glucose

To examine the response signal of the fabricated sensor, a chronoamperometry measurement was conducted in 50 mL of 0.1 M NaOH solution at a potential of 0.45 V. In a time interval of 50 s, 10 µL of 50 mM β-D-glucose solution was added to the NaOH solution.

The obtained data (as presented in Figure 9) showed that the response current increased significantly when the β-D-glucose solution was dropped into the working solution and reached a plateau after the β-D-glucose concentration in the system achieved a value of 0.4 mM. The increase in the response current was due to the occurrence of the redox reactions when the β-D-glucose solution was added to the electrochemical cell [36]. The mechanism of these redox reactions can be explained through the diagram presented in Figure 10. In this process, β-D-glucose molecules were oxidized to form gluconolactone, and Ce^{4+} ions were reduced to form Ce^{3+} ion. The results indicated that the fabricated CeO_2-based electrode could respond well to the presence of β-D-glucose in the solution without enzymes, proving that the electrode can be used as a nonenzymatic sensor for detecting β-D-glucose in a solution.

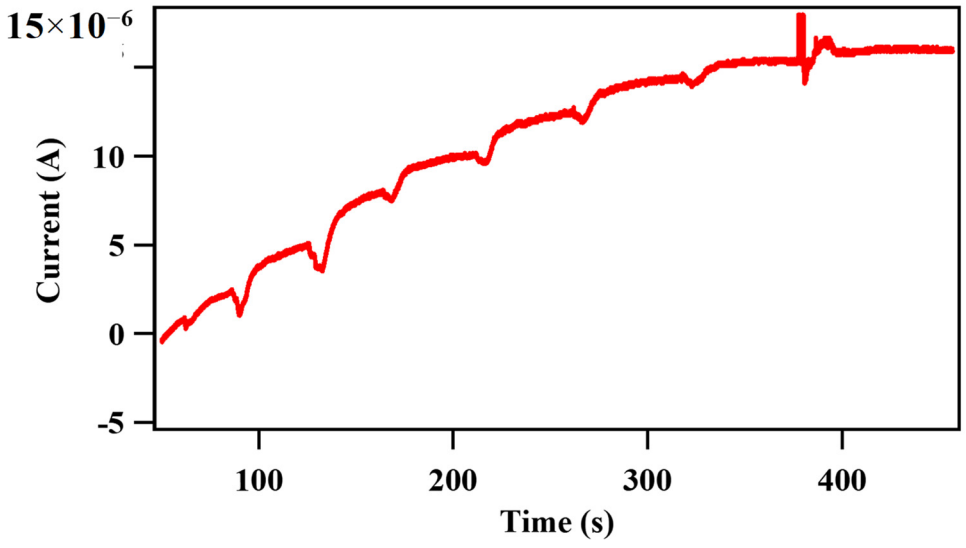

Figure 9. Chronoamperogram of the fabricated CeO_2 electrode in the 1 M NaOH solution, where 10 µL of 50 mM β-D-glucose was added in an interval time of 50 s.

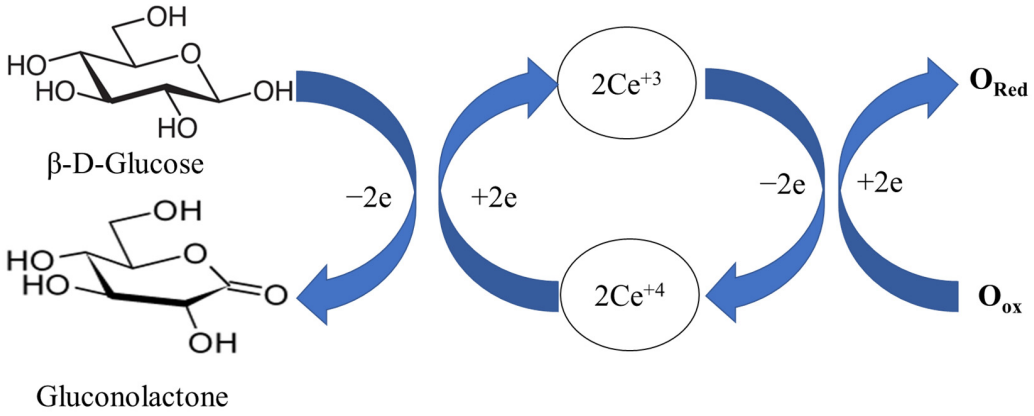

Figure 10. Oxidation mechanism of β-D-glucose on the surface of the sensor.

To test the dependence of the response signal of the sensor on the concentration of β-D-glucose, experiments were carried out using a conventional three-electrode cell in a solution of 0.1 M NaOH and β-D-glucose. The concentration of β-D-glucose was varied from 0.05 mM to 0.8 mM. The scanning mode was a linear mode with a scanning rate of 100 mV/s. Figure 11 shows the LSV curves obtained with different concentrations of β-D-glucose. It can be seen that when the concentration increased from 0.05 to 0.7 mM, the intensity of the response current increased. For a concentration of 0.8 mM, the intensity of the response current was close to that obtained in the 0.7 mM solution, indicating that the proper working concentration range was $\leq$0.7 mM.

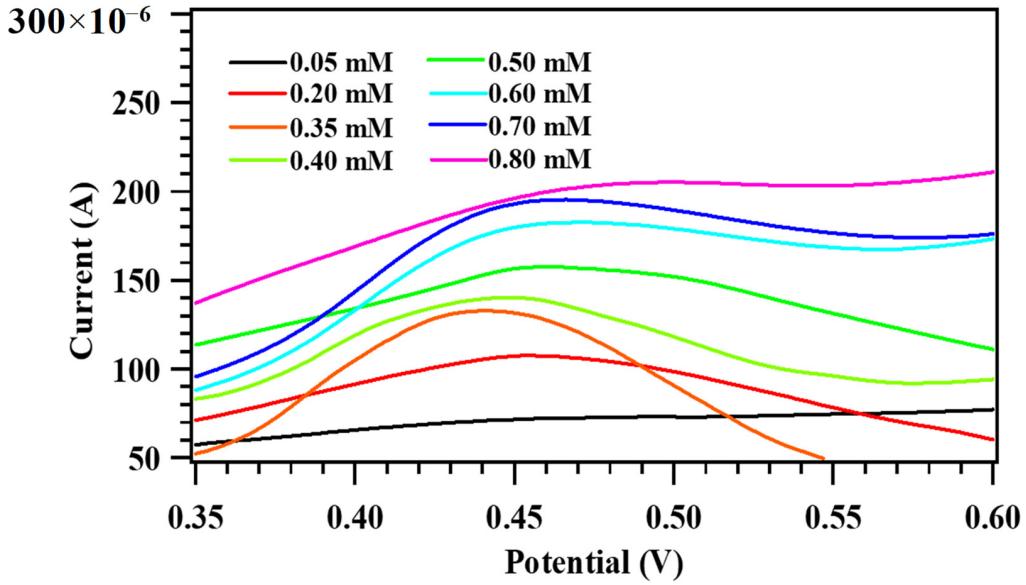

Figure 11. LSV curves of the fabricated sensor recorded at a scan rate of 100 mV/s in the solution containing 0.1 M NaOH and β-D-glucose with concentration varying from 0.05 mM to 0.80 mM.

To establish the calibration curve and determine the limit of detection (LOD) of the fabiricated sensor, experiments were conducted in a β-D-glucose concentration range of 0.05–0.7 mM. The experiments were triplicated to ensure reproductivity. As presented in Figure 12, the current intensity increased linearly with an increase in the β-D-glucose concentration from 0.05 to 0.70 mM. The correlation coefficient of the linear regression was 0.997, indicating a linear relationship between the current intensity (A) and the β-D-glucose concentration (mM) with the following equation: $I = 1.861 \times 10^{-4} \times C + 6.642 \times 10^{-5}$. The sensitivity of the glucose sensor was calculated from the calibration curve slope and divided by the electroactive working area of the sensor. The calculated sensitivity was

found to be 37.72 μA/mM·cm^2. The limit of detection (LOD) of the glucose sensor was observed to be 0.093 mM, and the standard error (SE) of the intercept was 1.997 × 10^{-6}.

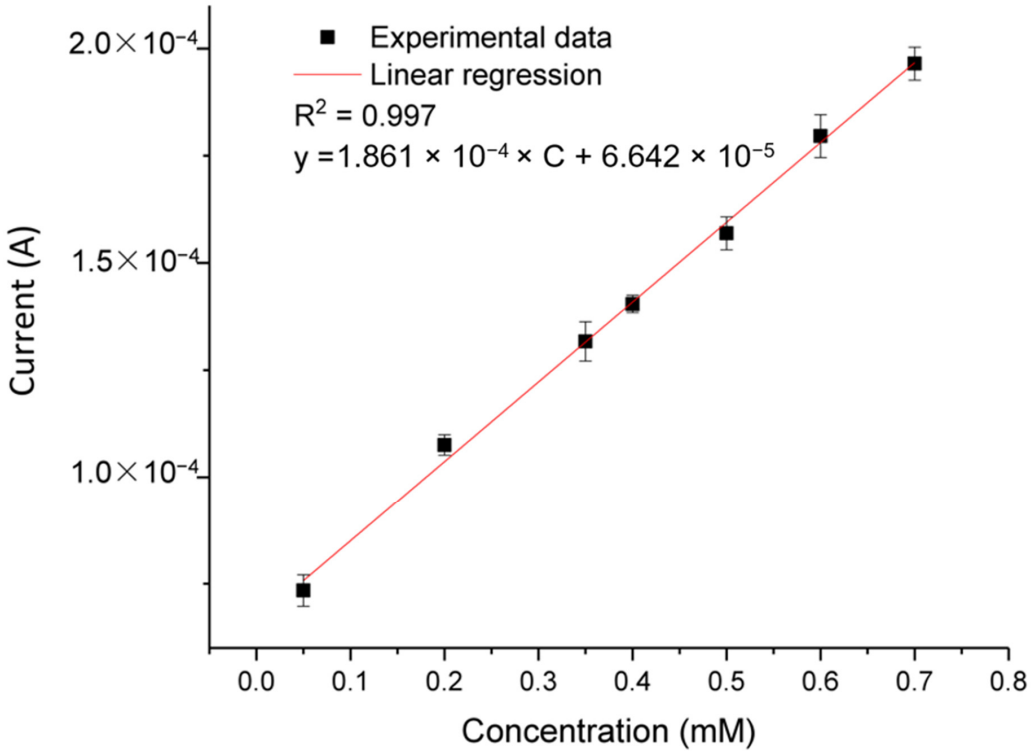

Figure 12. The calibration curve established in the concentration range of 0.05–0.7 mM at a potential of 0.45 V with a scan rate of 100 mV/s.

Experiments were carried out in the presence of ascorbic acid (AA) and uric acid (UA) in order to examine the selectivity of the fabricated sensor. Figure 13 shows the LSV curves of the sensors in a solution of 1 M NaOH and 0.1 mM β-D-glucose (a) and a solution containing 1 M NaOH, 0.1 mM glucose, 0.1 mM AA, and 0.1 mM UA (b).

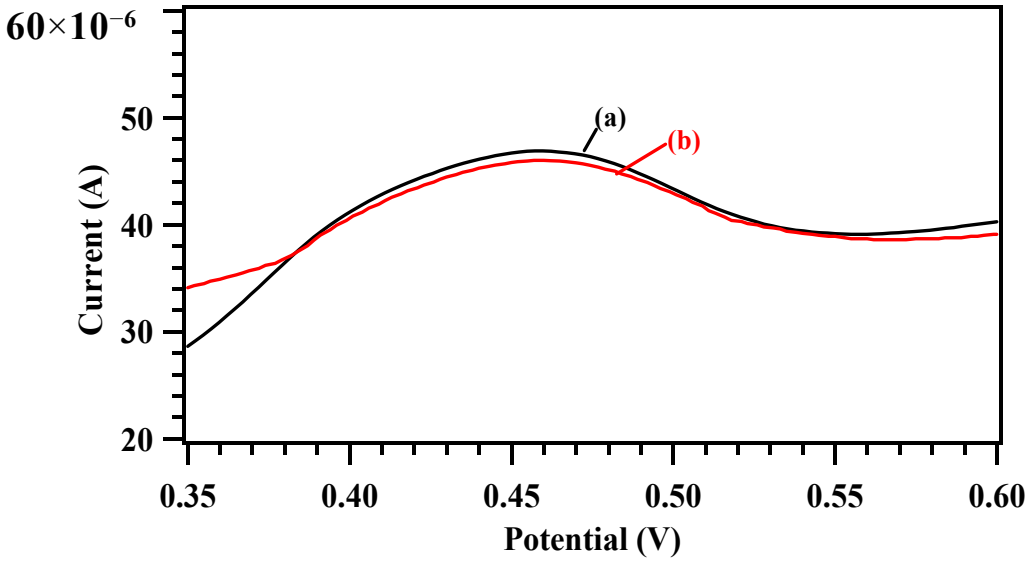

Figure 13. LSV curves of the fabricated sensor in the following solutions: (a) 1 M NaOH and 0.1 mM glucose; (b) 1 M NaOH, 0.1 mM glucose, 0.1 mM AA, and 0.1 mM UA.

The data showed that the signals of the sensor in these two cases were almost identical, indicating that the presence of AA and UA did not interfere with the glucose signal of the fabricated sensor. A chronoamperometry measurement was carried out in a solution of 1 M NaOH to test the selectivity further. During the measurement, after 100, 200, 300, 400, and 500 s, 100 µL of 0.1 mM β-D-glucose was added, and after 600 and 700 s, 100 µL of AA was added. The same amount of AA was also added to the system after 800 and 900 s. The results (Figure 14) showed that the intensity of the signal increased with an increase in the amount of β-D-glucose added to the system. When the AA and UA solutions were added to the system, the signal remained nearly unchanged, indicating that the fabricated sensor has a high selectivity to β-D-glucose and can be used for detecting glucose in a solution.

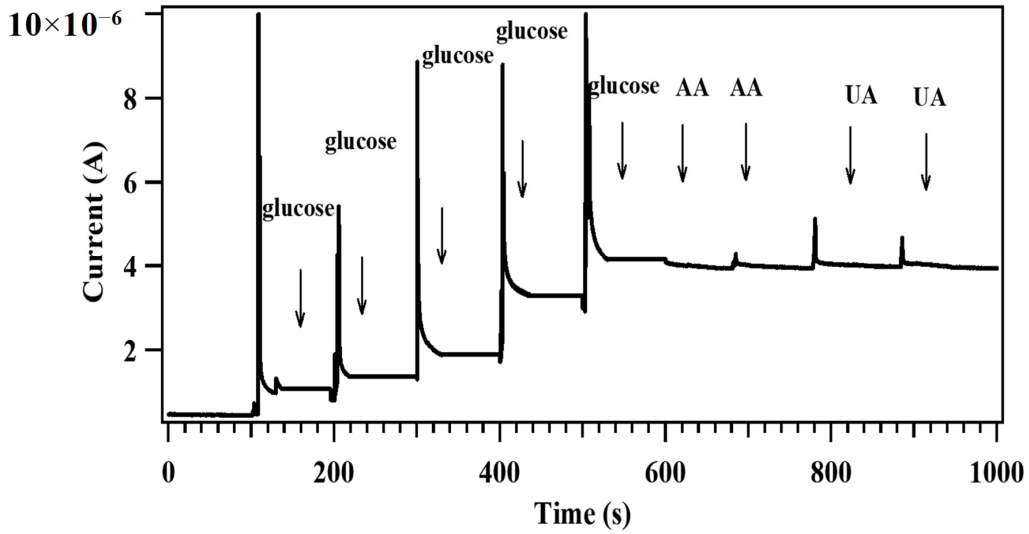

Figure 14. Chronoamperometry graph of the fabricated sensor in a 1 M NaOH solution whilst separately adding a solution of 0.1 mM β-D-glucose at 100, 200, 300, 400, and 500 s, 0.1 mM AA at 600 and 700 s, and 0.1 mM UA at 800 and 900 s.

4. Conclusions

A CeO_2 branched-like nanostructure on a Au/Si electrode surface was directly fabricated by electrodeposition at room temperature from a solution containing 0.015 M $Ce(NO_3)_3$, 0.01 M KCl, and 0.02 M CH_3COONH_4 with a scan rate of 400 mV/s. The formation of the CeO_2 branched-like nanostructure depended on the parameters, including the cyclic voltammetry, CH_3COOH content, and scan cycle number. The optimal conditions for the preparation of the CeO_2 branched-like nanostructure were a CH_3COOH content of 1 mL and a scan cycle number of 100. The fabricated electrode was used as a nonenzymatic biosensor for glucose detection. The feasibility of the sensor in terms of glucose detection was tested by chronoamperometry and cyclic voltammetry. The results indicated that the sensor's sensitivity was 37.72 µA/mM·cm^2, and the sensor's limit of detection (LOD) was 1.67 µM. The findings of this work indicate that a CeO_2 branched-like nanostructure can be directly fabricated and used for nonenzymatic biosensors.

Author Contributions: Conceptualization, N.T.N. (Nguyen Thi Nguyet) and C.V.T.; Validation, C.V.T., D.T.T.N. and N.T.N. (Nguyen Trong Nghia); Investigation, N.T.N. (Nguyen Thi Nguyet) and D.T.T.N.; Writing—original draft, N.T.N. (Nguyen Thi Nguyet) and P.D.T.; Writing—review & editing, C.V.T., P.D.T., V.D.N. and N.T.N. (Nguyen Trong Nghia); Visualization, D.T.T.N. and V.D.N. All authors have read and agreed to the published version of the manuscript.

Funding: This research was funded by Hung Yen University of Technology and Education under grant number UTEHY.L.2021.06.

Institutional Review Board Statement: Not applicable.

Informed Consent Statement: Not applicable.

Data Availability Statement: Data will be made available on request.

Conflicts of Interest: The authors declare no conflict of interest.

References

1. Liu, J.; Lang, Q.; Liang, B.; Zheng, Z.; Zhang, Y.; Liu, A. Sensitive Electrochemical Sequential Enzyme Biosensor for Glucose and Starch Based on Glucoamylase- and Glucose Oxidase-Controllably Co-Displayed Yeast Recombinant. *Anal. Chim. Acta* **2022**, *1221*, 340173. [CrossRef] [PubMed]
2. Wang, Q.; Chen, M.; Xiong, C.; Zhu, X.; Chen, C.; Zhou, F.; Dong, Y.; Wang, Y.; Xu, J.; Li, Y.; et al. Dual Confinement of High–Loading Enzymes within Metal–Organic Frameworks for Glucose Sensor with Enhanced Cascade Biocatalysis. *Biosens. Bioelectron.* **2022**, *196*, 113695. [CrossRef] [PubMed]
3. Güler, M.; Zengin, A.; Alay, M. Fabrication of Glucose Bioelectrochemical Sensor Based on Au@Pd Core-Shell Supported by Carboxylated Graphene Oxide. *Anal. Biochem.* **2023**, *667*, 115091. [CrossRef] [PubMed]
4. Bal Altuntaş, D.; Kuralay, F. MoS_2/Chitosan/GOx-Gelatin Modified Graphite Surface: Preparation, Characterization and Its Use for Glucose Determination. *Mater. Sci. Eng. B* **2021**, *270*, 115215. [CrossRef]
5. Li, B.; Wu, X.; Shi, C.; Dai, Y.; Zhang, J.; Liu, W.; Wu, C.; Zhang, Y.; Huang, X.; Zeng, W. Flexible Enzymatic Biosensor Based on Graphene Sponge for Glucose Detection in Human Sweat. *Surf. Interfaces* **2023**, *36*, 102525. [CrossRef]
6. Chavez-Urbiola, I.R.; Reséndiz-Jaramillo, A.Y.; Willars-Rodriguez, F.J.; Martinez-Saucedo, G.; Arriaga, L.G.; Alcantar-Peña, J.; Escalona-Villalpando, R.A.; Ledesma-García, J. Glucose Biosensor Based on a Flexible Au/ZnO Film to Enhance the Glucose Oxidase Catalytic Response. *J. Electroanal. Chem.* **2022**, *926*, 116941. [CrossRef]
7. Hassan, M.H.; Vyas, C.; Grieve, B.; Bartolo, P. Recent Advances in Enzymatic and Non-Enzymatic Electrochemical Glucose Sensing. *Sensors* **2021**, *21*, 4672. [CrossRef]
8. Hwang, D.-W.; Lee, S.; Seo, M.; Chung, T.D. Recent Advances in Electrochemical Non-Enzymatic Glucose Sensors—A Review. *Anal. Chim. Acta* **2018**, *1033*, 1–34. [CrossRef]
9. Lu, X.; Zheng, D.; Zhang, P.; Liang, C.; Liu, P.; Tong, Y. Facile Synthesis of Free-Standing CeO_2 Nanorods for Photoelectrochemical Applications. *Chem. Commun.* **2010**, *46*, 7721–7723. [CrossRef]
10. Yin, D.; Zhao, F.; Zhang, L.; Zhang, X.; Liu, Y.; Zhang, T.; Wu, C.; Chen, D.; Chen, Z. Greatly Enhanced Photocatalytic Activity of Semiconductor CeO_2 by Integrating with Upconversion Nanocrystals and Graphene. *RSC Adv.* **2016**, *6*, 103795–103802. [CrossRef]
11. Patel, R.L.; Palaparty, S.A.; Liang, X. Ultrathin Conductive CeO_2 Coating for Significant Improvement in Electrochemical Performance of $LiMn_{1.5}Ni_{0.5}O_4$ Cathode Materials. *J. Electrochem. Soc.* **2017**, *164*, A6236–A6243. [CrossRef]
12. Das, H.T.; Elango Balaji, T.; Dutta, S.; Das, N.; Das, P.; Mondal, A.; Imran, M. Recent Trend of CeO_2-Based Nanocomposites Electrode in Supercapacitor: A Review on Energy Storage Applications. *J. Energy Storage* **2022**, *50*, 104643. [CrossRef]
13. Muccillo, E.; Rocha, R.; Tadokoro, S.; Rey, J.; Muccillo, R.; Steil, M. Electrical Conductivity of CeO_2 Prepared from Nanosized Powders. *J. Electroceramics* **2004**, *13*, 609–612. [CrossRef]
14. Munirathnam, R.; Rumana Farheen, S.M.; Manjunatha, S.; Manjunatha, H.C.; Vidya, Y.S.; Sridhar, K.N.; Seenappa, L.; Veera Rethina Murugan, S.; Krishnaveni, S. Tulsi Mediated Green Synthesis of Zinc Doped CeO_2 for Super Capacitor and Display Applications. *J. Sci. Adv. Mater. Devices* **2023**, *8*, 100551. [CrossRef]
15. Dao, N.N.; Luu, M.D.; Nguyen, Q.K.; Kim, B.S. UV Absorption by Cerium Oxide Nanoparticles/Epoxy Composite Thin Films. *Adv. Nat. Sci. Nanosci. Nanotechnol.* **2011**, *2*, 045013. [CrossRef]
16. Bao, B.; Sun, Y.; Li, X.; Li, L.; Yu, Y. Tuning the UV Absorbing Ability of CeO_2 Nanoparticles with F—Doping. *FlatChem* **2023**, *39*, 100494. [CrossRef]
17. Laubender, E.; Tanvir, N.B.; Yurchenko, O.; Urban, G. Nanocrystalline CeO_2 as Room Temperature Sensing Material for CO_2 in Low Power Work Function Sensors. *Procedia Eng.* **2015**, *120*, 1058–1062. [CrossRef]
18. Renganathan, B.; Krishna Rao, S.; Ganesan, A.R.; Deepak, A. Investigating the Gas Sensing Potential in CeO_2 Fiber Optic Sensor via Trivalent Gadolinium Ion Substitution at Room Temperature. *Mater. Lett.* **2022**, *325*, 132766. [CrossRef]
19. Guan, P.; Li, Y.; Zhang, J.; Li, W. Non-Enzymatic Glucose Biosensor Based on CuO-Decorated CeO_2 Nanoparticles. *Nanomaterials* **2016**, *6*, 159. [CrossRef]
20. Nguyet, N.T.; Hai Yen, L.T.; Van Thu, V.; lan, H.; Trung, T.; Vuong, P.H.; Tam, P.D. Highly Sensitive DNA Sensors Based on Cerium Oxide Nanorods. *J. Phys. Chem. Solids* **2018**, *115*, 18–25. [CrossRef]
21. Solanki, P.R.; Ali, M.A.; Kaushik, A.; Malhotra, B.D. Label-Free Capacitive Immunosensor Based on Nanostructured Cerium Oxide. *Adv. Electrochem.* **2014**, *1*, 92–97. [CrossRef]
22. Tam, P.D.; Thang, C.X. Label-Free Electrochemical Immunosensor Based on Cerium Oxide Nanowires for Vibrio Cholerae O1 Detection. *Mater. Sci. Eng. C* **2016**, *58*, 953–959. [CrossRef] [PubMed]
23. Nguyet, N.T.; Yen, L.T.H.; Doan, V.Y.; Hoang, N.L.; Van Thu, V.; Lan, H.; Trung, T.; Pham, V.H.; Tam, P.D. A Label-Free and Highly Sensitive DNA Biosensor Based on the Core-Shell Structured CeO_2-NR@Ppy Nanocomposite for Salmonella Detection. *Mater. Sci. Eng. C* **2019**, *96*, 790–797. [CrossRef] [PubMed]
24. Yang, X.; Yu, X.; Li, G. The Effects of Nd Doping on the Morphology and Optical Properties of CeO_2 Nanorods. *J. Mater. Sci. Mater. Electron.* **2016**, *27*, 9704–9709. [CrossRef]

25. Li, G.; Lu, X.; Zhao, W.; Su, C.; Tong, Y. Controllable electrochemical synthesis of Ce^{4+}-doped ZnO nanostructures from nanotubes to nanorods and nanocages. *Cryst. Growth Des.* **2008**, *8*, 1276–1281. [CrossRef]
26. Lu, X.; Zheng, D.; Gan, J.; Liu, Z.; Liang, C. Porous CeO2 Nanowires/Nanowire Arrays: Electrochemical Synthesis and Application in Water Treatment. *J. Mater. Chem.* **2010**, *20*, 7118–7122. [CrossRef]
27. Zhang, C.; Zhang, X.; Wang, Y.; Xie, S.; Liu, Y. Facile Electrochemical Synthesis of CeO_2 Hierarchical Nanorods and Nanowires with Excellent Photocatalytic Activities. *New J. Chem.* **2014**, *28*, 2581–2586. [CrossRef]
28. Ho, P.H.; Ambrosetti, M.; Groppi, G.; Tronconi, E.; Fornasari, G.; Vaccari, A.; Benito, P. Electrodeposition of CeO_2 and Pd-CeO_2 on Small Pore Size Metallic Foams: Selection of Deposition Parameters. *Catal. Today* **2019**, *334*, 37–47. [CrossRef]
29. Feng, Z.; Ren, Q.; Peng, R.; Mo, S.; Zhang, M.; Fu, M.; Chen, L.; Ye, D. Effect of CeO_2 Morphologies on Toluene Catalytic Combustion. *Catal. Today* **2019**, *332*, 177–182. [CrossRef]
30. Nguyet, N.T.; Trung, T.; Lan, H.; Van Thu, V.; Vuong, P.H.; Tam, P.D. Direct Synthesis of CeO_2 Nanospindles on Gold Electrode by Electrochemical Method. *Vietnam J. Chem.* **2019**, *57*, 57–63. [CrossRef]
31. Bard, A.J.; Faulkner, L.R.; White, H.S. *Electrochemical Methods: Fundamentals and Applications*; John Wiley & Sons: Hoboken, NJ, USA, 2022; ISBN 1119334063.
32. Pradhan, D.; Reddy, R.G. Mechanistic Study of Al Electrodeposition from EMIC-$AlCl_3$ and BMIC-$AlCl_3$ Electrolytes at Low Temperature. *Mater. Chem. Phys.* **2014**, *143*, 564–569. [CrossRef]
33. Wang, Q. Anodic Electrochemical Synthesis and Characterization of Nanocrystalline Cerium Oxide and Cerium Oxide/Montmorillonite Nanocomposites. Ph.D. Dissertation, University of North Texas, Denton, TX, USA, 2014.
34. Sabari Arul, N.; Mangalaraj, D.; Kim, T.W.; Chen, P.C.; Ponpandian, N.; Meena, P.; Masuda, Y. Synthesis of CeO_2 Nanorods with Improved Photocatalytic Activity: Comparison between Precipitation and Hydrothermal Process. *J. Mater. Sci. Mater. Electron.* **2013**, *24*, 1644–1650. [CrossRef]
35. Kumar, A.M.; Babu, R.S.; Ramakrishna, S.; de Barros, A.L.F. Electrochemical Synthesis and Surface Protection of Polypyrrole-CeO_2 Nanocomposite Coatings on AA2024 Alloy. *Synth. Met.* **2017**, *234*, 18–28. [CrossRef]
36. Dinh Van, T.; Dang Thi Thuy, N.; Dao Vu Phuong, T.; Nguyen Thi, N.; Nguyen Thi, T.; Nguyen Phuong, T.; Vu Van, T.; Vuong-Pham, H.; Phuong Dinh, T. High-Performance Nonenzymatic Electrochemical Glucose Biosensor Based on AgNP-Decorated MoS_2 Microflowers. *Curr. Appl. Phys.* **2022**, *43*, 116–123. [CrossRef]